IEEE Access
Multidisciplinary | Rapid Review | Open Access Journal

Received February 14, 2021, accepted March 3, 2021, date of publication March 9, 2021, date of current version March 29, 2021.

Digital Object Identifier 10.1109/ACCESS.2021.3064600

Intensity Modulated Gas RI Sensor Based on Inornate Antiresonant Hollow-Core Fiber With Ultrahigh Sensitivity

MAOXIANG HOU, NENG WANG, JIANGUO MA, YUN CHEN, AND XIN CHEN, (Member, IEEE)
State Key Laboratory of Precision Electronic Manufacturing Technology and Equipment, Guangdong University of Technology, Guangzhou 510006, China
Corresponding author: Yun Chen (chenyun@gdut.edu.cn)

This work was supported in part by the Key-Area Research and Development Program of Guangdong Province under Grant 2018B090906002; in part by the National Natural Science Foundation of China under Grant 61905044, Grant U1913212, and Grant 61875128; and in part by the Natural Science Foundation of Guangdong Province under Grant 2019A1515010895 and Grant 2019A1515011393.

ABSTRACT A gas refractive index (RI) sensor based on an inornate antiresonant hollow-core fiber (HCF) was theoretically analyzed and experimentally demonstrated. The transmission spectra evolution of the proposed sensor and the resonance intensity variations to the surrounding gas RI were simulated. Theoretical analysis found that the intensity sensitivity of inornate HCF is higher than that of coated HCF. In the experiment, a sensor with a 5 mm-long HCF provided exceptional sensitivity—as high as 2236.1 dB/RIU. The sensitivity was enhanced by improving the resonance intensity of the inornate HCF, which could be further improved by increasing the HCF length. In addition, temperature sensing was performed to resolve the temperature cross-sensitivity issue using a wavelength interrogation method. The proposed RI sensor exhibited the advantages of easily manufactured and with ultrahigh sensitivity.

INDEX TERMS Gas refractive index sensing, antiresonant mechanism, hollow-core fiber.

I. INTRODUCTION

The refractive index (RI) of a gas is seen as a gauge of information such as its concentration, type, and optical properties, which are of great significance in the petrochemical industry [1], gas lasing systems [2] and environmental monitoring [3]. Numerous fiber-optic sensors have been proposed for RI detection, such as modal interferometer [4], opened-cavity Mach-Zehnder interferometer [5], fiber surface plasmon resonance sensor [6], trench-embedding fiber taper [7], long-period grating [8], [9], and tilted fiber Bragg grating [10]. Most RI sensors are designed for an aquatic environment, that the RI measurement region is approximately 1.33. Gas detection has an external RI of ∼1.0, which should overcome the larger mismatch between the allowable guided mode and the external gaseous medium [11]. There are a few reports regarding gas RI sensing, which use the wavelength demodulation method to achieve the highest wavelength sensitivity. A gas RI sensor based on an open-cavity Fabry–Perot interferometer combined with the Vernier effect obtained a typical sensitivity of 30,899 nm/RIU [12]. By operating a microfiber modal interferometer at the dispersion turning point, an exceptional sensitivity of 69,984.3 nm/RIU can be obtained in [13]. By using a nanofiber couple, the sensitivity was enhanced even more up to 92,020 nm/RIU [14]. By employing a microfiber-based Sagnac interferometer at the group birefringence turning point, the highest RI sensitivity reached 160,938.9 nm/RIU [11]. However, temperature cross-sensitivity is a key issue because the higher the sensitivity, the more susceptible the sensor was to the external environment, resulting in poor measurement accuracy. Moreover, the complicated configuration and fragile structure of the above sensors limit their practical implementation and their potential for mass production. In this regard, reliable gas RI sensors with high sensitivity, accuracy, and cost-effectiveness are in great demand in real-world applications.

Antiresonant (AR) mechanism-based hollow-core fiber (HCF) has attracted a great deal of attention in recent years owing to its transmission spectrum containing periodic high visibility spectral dips. AR-based HCF has the simplest single-layer cladding structure and offers extraordinary

The associate editor coordinating the review of this manuscript and approving it for publication was Aijun Yang.

advantages in the sensing fields [15]. A functionalized colloid has been filled in the air core of an HCF to increase its temperature sensitivity [16]. Many functional films coated on the surface of an HCF have been demonstrated in a wide range of applications in humidity [17], temperature [18], twist [19], curvature [20], displacement [21], and gas RI [22], [23]. The HCF can also be preprocessed through a femtosecond laser drilling hole to detect the outside air pressure [24], [25]. However, these sensors require elaborate processes, such as film thickness control and, femtosecond micromachining, which seriously restrict mass production and application.

In this letter, we demonstrate a gas RI sensor using an AR-based inornate HCF, which can achieve an ultrahigh sensitivity when interrogating the intensity of the transmission resonance dips. Firstly, we theoretically analyzed and simulated the transmission spectra evolution of the proposed sensor and its resonance intensity variations to the surrounding RI. The deeper the visibility is, the higher the sensitivity. The intensity sensitivity of inornate HCF is higher than that of coated HCF. Secondly, we experimentally investigated the RI response of sensors with different HCF lengths using an intensity interrogation method. The gas RI sensitivity of a 5 mm-length HCF sensor reached up to 2236.1 dB/RIU in the range of 1 to 1.002. At the same time, we found that the sensitivity was proportional to the length of the HCF, and could be sufficiently enhanced. A temperature sensitivity of 26.4 pm/°C was obtained experimentally, and the temperature cross-sensitivity of the sensor could be resolved through different interrogation methods. Moreover, the proposed sensor exhibited a simple production process, and making it beneficial to large-scale manufacturing with great potential for chemical applications.

II. SENSING PRINCIPLE AND SIMULATION RESULTS

As mentioned in our previous work [25], a section of an HCF of length of L was spliced between two sections of a commercial single mode fiber (SMF, G652.d YOFC Co., Ltd., Wuhan, China), then measured its transmission spectrum to sensing the surrounding environment. The applied HCF is a pure silica hollow fiber (Polymicro Technologies, model TSP025150, Phoenix, Arizona, USA) with an inner radius of 12.5 μm (r), a cladding thickness of 50 μm (d), and an outer diameter of 125 μm (D), as shown in Fig. 1(a). It is well known that the optical guiding mechanism of a HCF can be explained according to the antiresonant reflecting optical waveguide (ARROW) model [26] (also known as multiple beam interferences in the cladding of HCF). Its optical properties are mainly determined by the thickness of the high RI cladding layer, which is considered to be a Fabry-Perot etalon. When the frequency of light satisfies the resonance condition of the cladding, the light will leak out of the HCF, as shown by the t_2 arrow in Fig. 1(b), and the light that does not satisfy the resonance condition will be bound, and propagate forward in the hollow core, as shown by the r_1 arrow in Fig. 1(b). In the ARROW model, the resonant

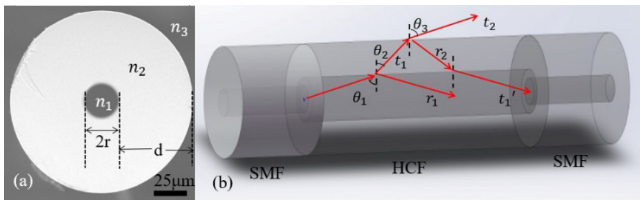

FIGURE 1. (a) Cross-sectional optical image of the employed HCF. (b) Schematic diagram of the proposed sensor with structure and optical pathways.

wavelength λ_m can be expressed as [27]:

$$\lambda_m = \frac{2d}{m}\sqrt{n_2^2 - n_1^2 sin\theta_1^2}. \tag{1}$$

where d=50 μm, $n_2 n_1 = 1$ (under normal pressure), and m is an integer beginning with 1. θ_1 is the incident angle, and taken as pi/2 at the resonance condition.

As shown in Fig. 1(b), the HCF cladding can be viewed as a Fabry-Perot etalon [26]. The amplitude of the incident light is A_i, the light is incident from the air core into the cladding, with a reflection coefficient of r_1, a refraction coefficient of t_1 and an incident angle of $\boldsymbol{\theta_1}$. The light is transmitted from the cladding n_2 to the outside surroundings n_3. The reflection coefficient at the outer interface of the cladding is r_2. According to the principle of multi-beam interference, the complex amplitude of the reflected light is:

$$A_r(\delta) = \frac{A_i\left(r_1 + r_2 e^{i\delta}\right)}{1 + r_1 r_2 e^{i\delta}}. \tag{2}$$

In the above equation, δ is the phase difference between two adjacent reflected lights (namely r_1 and t_1' in Fig. 1(b)), and its expression is

$$\delta = \frac{4\pi d n_2 cos_{\theta_2}}{\lambda}. \tag{3}$$

Then, the reflected light intensity can be derived as:

$$I_R = A_R A_R^* = \frac{r_1^2 + r_2^2 - 2r_1 r_2 cos\delta}{1 + r_1^2 r_2^2 - 2r_1 r_2 cos\delta} I_0, \tag{4}$$

where I_0 is the incident light intensity. Therefore, the total reflectance R of the cladding layer is

$$R = \frac{r_1^2 + r_2^2 - 2r_1 r_2 cos\delta}{1 + r_1^2 r_2^2 - 2r_1 r_2 cos\delta}. \tag{5}$$

The reflection coefficients r_1 and r_2 are determined by the Fresnel reflection formula (TE polarization as an example):

$$r_1 = \frac{n_2 cos_{\theta_2} - n_1 cos_{\theta_1}}{n_1 cos_{\theta_1} + n_2 cos_{\theta_2}}, \tag{6}$$

$$r_2 = \frac{n_3 cos_{\theta_3} - n_2 cos_{\theta_2}}{n_2 cos_{\theta_2} + n_3 cos_{\theta_3}}. \tag{7}$$

The dispersion of the cladding n_2 was included in these calculations by using the Sellmeier equation for fused silica. Suppose P is the power along the propagation direction of HCF, we have [15]:

$$T(\lambda) = \frac{P_{z=L}}{P_{z=0}} = R^N. \tag{8}$$

where L is the propagation distance and N is the number of apex points in the zigzag representing the ray trajectory per length L, can be expressed as

$$N = \frac{L}{2r * tan\theta_1}. \tag{9}$$

In the core region, the incidence angle θ_1 of the propagation mode (fundamental mode) has an effective index n_{eff}, which is defined as

$$sin\theta_1 = \frac{n_{eff}}{n_1}. \tag{10}$$

The effective index n_{eff} of the fundamental mode of HCF are simulated through a full-vector finite-element method [21]. Using the structural parameters of the used HCF, and considering the material dispersion of background silica, the n_{eff} of the fundamental mode at 1490.88 nm can be calculated as 0.999005, as shown in the inset of Fig. 3(b).

After calculating the incident angle θ_1 from the modal index n_{eff}, the transmission spectrum of the HCF T (λ) can be simulated using Eqs. (2) to (10). The normalized transmission spectra of the HCF in logarithmic coordinates are shown in Fig. 2(a), with $r = 12.5\ \mu m$, $d = 50\ \mu m$ and L=2 mm as an example. As shown in Fig. 2(a), the calculated resonant wavelengths λ_m according to the F-P theory were consistent with the calculated results from Eq. (1). As n_3 increased from 1 to 1.006, the reflectivity of the cladding R increased, resulting in an obvious intensity increased at the resonance dip. Moreover, no significant wavelength shift was observed. In the non-resonant region of the transmission spectra, there was almost no transmission loss at first (that is, the initial transmission intensity is 0 dB). As n_3 increases, the transmission intensity gradually reduced slightly, as shown in Fig. 2(a). Note that the transmission loss is ignored in the calculation and should be considered in the actual transmission tests. Since the single-layer ring cladding has a limited ability to confine the light field for transmission [15].

When $\delta = 2m\pi$, namely, the incident light meets the resonant condition, the transmission intensity T (λ_m) at the resonant wavelength λ_m is obtained. As shown in Fig. 2(b), T (λ_m) for HCF length of L = 1.5, 2, 4 and 5 mm appears to increase in logarithmic form. Moreover, the longer the length L, the more drastic its intensity changes, within the unit refractive index range, in other words, the longer the length, the greater the sensitivity. Note that the calculated dynamic range of T (λ_m) is very large, from negative infinity to −50 dB, which is far beyond the dynamic range of the optical spectrum analyzer (OSA, Yokogawa AQ6370C, Tokyo, Japan) we used (78 dB). So that, in actual applications, the transmission spectrum will be tested with a fixed and limited dynamic range, which is far away from the simulation result in Fig. 2. However, the trend of the simulation results should consistent with measured data. Moreover, we can infer that for the inornate HCF of a single-layer cladding, the greater the resonance intensity (the deeper the visibility), the higher the response sensitivity to the external gas RI.

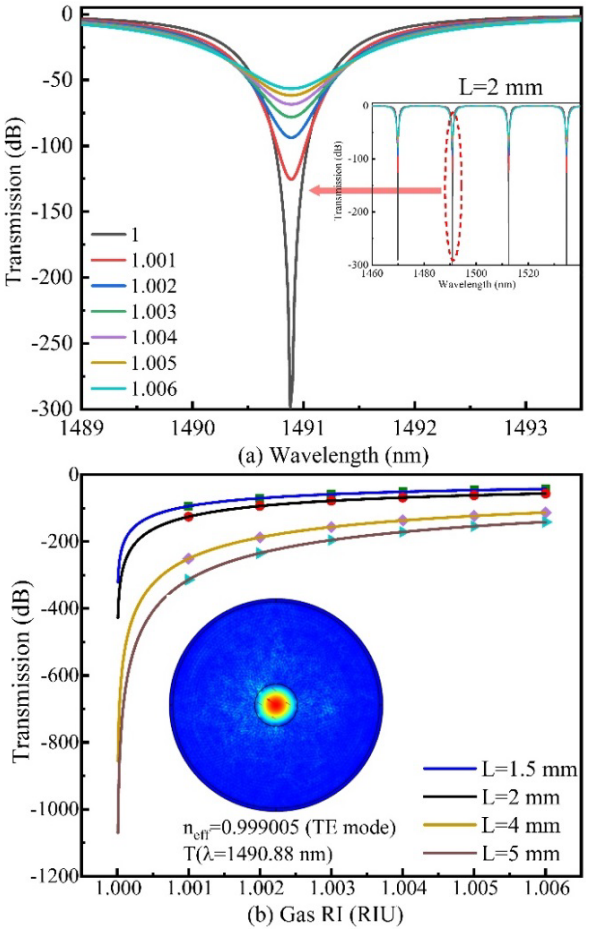

FIGURE 2. (a) Zoomed-in view of intensity changes various with the Gas RI. Inset: Calculated transmission spectra of HCF with $r = 12.5\ \mu m$, $d = 50\ \mu m$ and L=2 mm. (b) Calculated normalized intensity P_L/P_0 for HCF with $r = 12.5\ \mu m$, $d = 50\ \mu m$ and length of L = 1.5, 2, 4 and 5 mm, respectively, with respect to n_3 at 1490.88 nm. Inset: The mode field of the air core fundamental mode at 1490.88 nm.

Functional coatings have very large applications in optical fiber sensing. Generally, coatings can significantly expand the detection fields of silica optical fiber sensors and improve the sensing sensitivity. Similarly, when a functional film is coated on the outer surface of AR-HCF, its contrast, resonance wavelength and gas RI response to surrounding environment will also change. To this end, we built a double-layer membrane model. A functional film is coated outside of the cladding of HCF, as shown in Fig.3, whose refractive index is n_3, thickness is d_3, and the response of the coated HCF to external gas RI is analyzed. Ref. [26] shows that the resonant wavelength is determined by the two layers, which can be expressed as

$$\lambda_m = \frac{2}{m}(d\sqrt{n_2^2 - n_1^2 sin\theta_1^2} + d_3\sqrt{n_3^2 - n_1^2 sin\theta_1^2}) \tag{11}$$

Similarly, the reflectance of the double-layer film can be calculated by equivalent to a single-layer film using Eq. (5).

Accordingly, we calculated the transmission spectra and resonance dips changes of the HCF coating with different thicknesses films (L = 2 mm), divided into n_3 is less

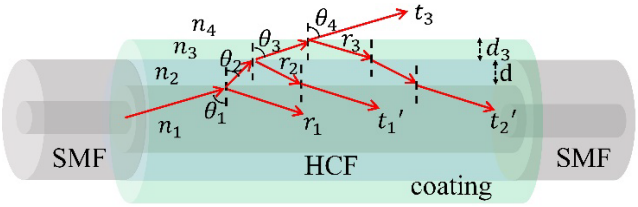

FIGURE 3. Schematic diagram of the double-layer cladding sensor with structure and optical pathways.

than n_2 (like 1.33) and n_3 is greater than n_2 (like 1.57). The refractive index of aquatic environments to be measured is approximately 1.33. The commonly used as functional film materials such as Polystyrene and PET have a refractive index around 1.57. As shown in Fig. 4 (a), when the refractive index n_3 of the coating is 1.33 and the thickness d_3 is 100, 372.5 and 650 nm, respectively, the resonance intensity is −56.8, −78.0 and −65.3 dB, respectively. Among them, the maximum is with a thickness of 372.5 nm. Also, in Fig. 4 (b), when the refractive index n_3 of the coating is 1.57 and the thickness d_3 is 100, 372.5 and 650 nm, respectively, the resonance intensity is −87.0, −113.4 and −79.9 dB, respectively. Also, the maximum is with a thickness of 372.5 nm. It is worth noting that all the above resonance dips are much shallower than the inornate HCF of a single-layer cladding (negative infinity, as shown in Fig. 2 (b)).

According to the enhancement reflection film theory, when d_3 is a quarter of the resonance wavelength, the reflectivity has the maximum value. As shown in the insets of Fig. 4, with the external gas RI increases, the visibility of resonance dips gradually weakens, change as a logarithmic form. This is consistent with the single-layer inornate HCF. From Fig. 4, we can find that the resonance intensities with coating are decrease slowly compared with the inornate HCF. Since the refractive index of the coating has an effect on the resonance visibility. The deeper the visibility is, the greater the changes in the unit refractive index, and the higher the sensitivity. Therefore, it is advisable to not coating functional film for HCF gas RI sensing.

It is important to discuss the structural deformation and stress distributions over the silica cladding region under an increased gas pressure. According to Eq. (3) and Eq. (5), the changes of these two parameters, namely the thickness d and the refractive index n_2 of the cladding, will affect the transmission spectrum of the HCF. To evaluate these changes, asingle-layer elasticity model of the silica cladding is established in ANSYS. The simulation results under the applied pressure of 20 bar are displayed in Fig. 5. The maximumdeformation happens near the outer edge of the cladding, is about −1.5e-6 mm (−1.5 nm) and the maximum stress happens near the inner wall of the hollow-core, is about 4.415 MPa, as shown in Fig. 5. Then, the refractive index of the silica cladding will be modified due to strain-optic effect. The stress-optic coefficients of silica are $C_1 = -6.9 \times 10^{-13}\text{m}^2/\text{N}$, and $C_2 = -41.9 \times 10^{-13}\ \text{m}^2/\text{N}$. The changes of the silica refractive index are estimated through the stress

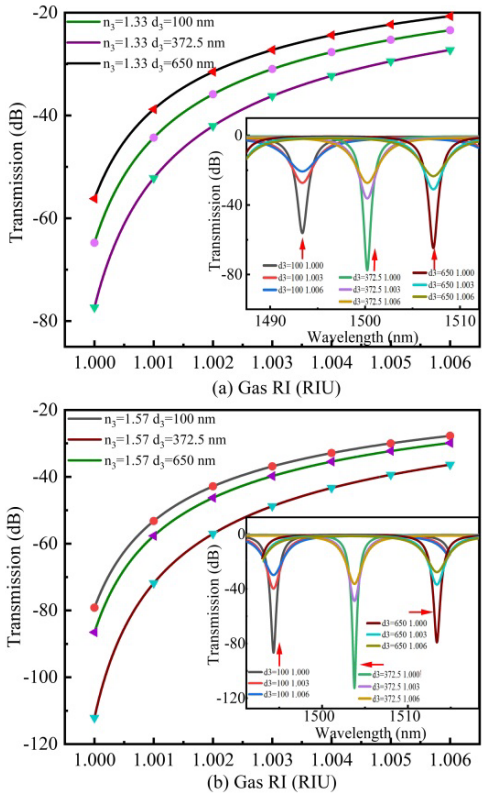

FIGURE 4. The function of calculated normalized intensity P_L/P_0 with respect to gas RI at resonant wavelength. The HCF coated a film with RI of (a) 1.33 and (b) 1.57 with thickness of 100, 372.5 and 650 nm, respectively. Inset: corresponding calculated transmission spectra of the coated HCF various with the Gas RI.

distribution in the cross section of the HCF [28], [29]. Using the maximum value 4.415 MPa, the maximum refractive index changes occur in the inner surface of the cladding with a value of $\sim 2.15 \times 10^{-5}$. By importing the calculated results into Eq. (8), the maximum deformation −1.5 nm, which will induce the resonant wavelength λ_m shifts about −0.05 nm. On the contrary, the maximum refractive index changes $\sim 2.15 \times 10^{-5}$, which will induce λ_m shifts about +0.043 nm. Both of these only change the resonance wavelength, and the results are opposite, so that they can counteract each other. The final combined effect is very small. At the same time, both of them have no effect on the intensity of the transmission spectrum, so the deformation and stress induced by gas pressure on the sensor can be ignored.

III. SENSING TESTS AND RESPONSE

Four HCF sensors of different lengths L, *i.e.* 1.5, 2, 4, and 5 mm, respectively, were fabricated through a simple fusion splicing process. The transmission spectra of the proposed sensors were measured using a wideband light source (1250-1650 nm, Shenzhen Fiber Lake Technology Co., Ltd., Shenzhen, China) and an OSA with a dynamic range of 78 dB, as shown in Fig. 6(a) to Fig. 6(d). Each sensor displayed five periodic dips in the range of 1450-1550 nm. The dip wavelengths λ_m exhibited slight deviations of approximately ±1 nm. In addition, these four sensors exhibited

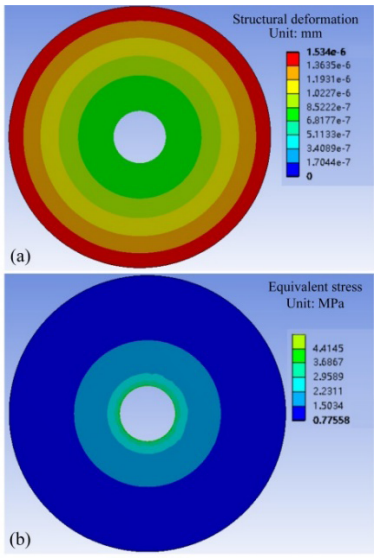

FIGURE 5. (a) Structural deformation distribution contours on the cross section of HCF with 20 bar air pressure. (b) Equivalent stress distribution contours on the cross section of HCF.

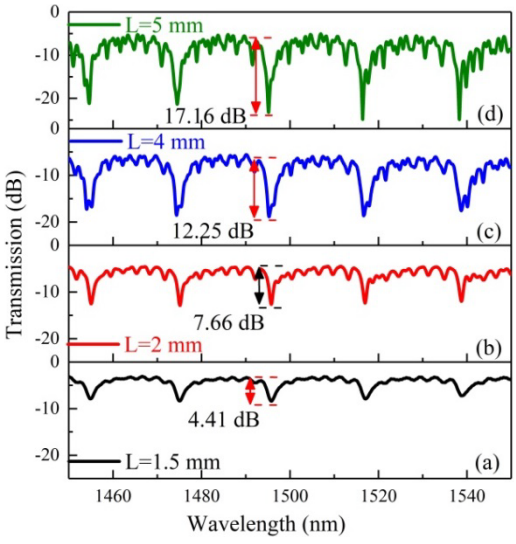

FIGURE 6. Measured transmission spectra of four fabricated sensors with different HCF lengths, i.e. 1.5 mm, 2 mm, 4 mm, and 5 mm, respectively.

minute differences from the calculated results of Eq. (1). This was most likely caused by the cladding thickness being not strictly uniform. Since a thickness error of 0.1 μm can shift the resonant wavelength ~3 nm.

The dip visibilities of the four sensors were 4.41, 7.66, 12.25, and 17.16 dB, respectively, as shown in Fig. 6. The transmission losses of the four sensors were −3.5, −4.8, −5.48, and −7.93 dB, respectively. As previously reported [15], the single-ring HCF exhibits a lesser ability to confine the light field, resulting in a relatively large transmission loss, which makes it unsuitable for long-distance optical transmission, but suitable for short-distance sensing. It should be noted that both dip visibility and transmission loss accumulate along the length of the HCF. Therefore, to maintain a steady sensing signal, the length of the HCF should be controlled within a few millimeters.

The RI of standard air (15~25 °C) is a function of the air pressure P (Pa) and temperature T (°C) [30]:

$$n_{air} = 1 + \frac{2.8793 * P * 10^{-9}}{1 + 0.00367 * T}. \tag{12}$$

When n_{air} (namely n_3) varies with pressure, the reflection coefficient of the cladding-air interface r_2 changes, and the transmission intensity T (λ) changes accordingly. Thus, the HCF can be used as a sensor for the detection of gas RI.

The air RI responses corresponding to the air pressure tests of the proposed sensors were investigated in a sealed air chamber, with a barometric generator and a high-precision pressure meter, as mentioned in [25]. The above four fabricated sensors with HCF lengths of 1.5, 2, 4, and 5 mm, respectively, were placed into the air chamber for the air RI tests. All tests were performed at a constant temperature (25°). The gas pressure in the chamber was increased from atmospheric pressure (1 bar) to 21 bar in steps of 1 bar, corresponding to the air RI increased from 1 to 1.0052 in increments of 0.00026. To ensure the accuracy of each test, the spectra were recorded after the air pressure was stabilized for 5 min.

Variations in the transmission spectra of the proposed sensors along with increasing the surrounding RI n_3 are shown in Fig. 7(a) to Fig. 7(d). As n_3 increased, the dip

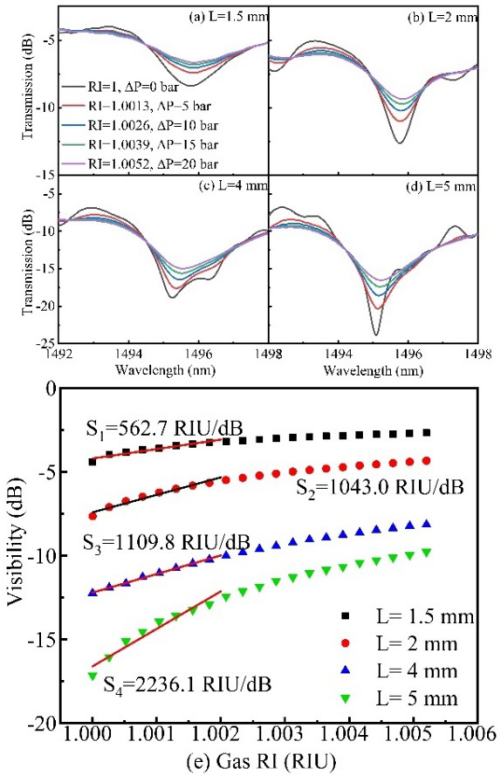

FIGURE 7. (a)-(d) Transmission spectra evolution of the proposed sensors as a function of the surrounding refractive index n_3. (e) The resonance dips visibility changes of four proposed sensors.

intensity $T(\lambda_m)$ at the resonance wavelength gradually increases, but the wavelength hardly shifted. In the non-resonant region, the spectral intensity decreased slightly. This was consistent with the calculation results shown in Fig. 2(a). To eliminate the impact of the transmission loss of the HCF, the dip visibility changes as functions of n_3 are shown in Fig. 7(e). The variations in the visibility of each dip are shown in logarithmic form, and the variation trend is consistent with the theoretical results of Fig. 2(b). Noting that, under a fixed and limited dynamic range, the measured values are different from theoretical results. In the range of n_3 from 1-1.002, the visibility changed sharply, while in the range greater than 1.002, the visibility changed slowly. In the range of 1-1.002, the linear fitting sensitivities of the above four sensors are 562.7, 1,043.0, 1,109.8, 2,236.1 dB/RIU, respectively. The sensitivity of the inornate HCF sensor was more than an order of magnitude larger than that of tilted fiber Bragg grating based sensor [10], four times larger than that of grapheme film-coated HCF [22], and five times larger than that of the parabolic-cylinder-like long-period fiber grating sensor [8]. Moreover, the air RI sensitivity of the proposed sensors was proportional to the HCF length L, which could be further improved. It should be noted that the maximum HCF length was limited by the transmission loss.

The influence of temperature on the proposed inornate HCF sensor (L=*5 mm*) was also investigated in a home-made oven over the range of 20-500 °C in increments of 100 °C. The corresponding transmission spectra are shown in the inset of Fig. 8, with an obvious red-shift process. A linear fitted wavelength sensitivity of S_T=26.4 *pm/°C* is shown in Fig. 8. Furthermore, the dip (around 1490 nm) intensity presents very little changes with temperature, the variation range was within ±1 dB, without obvious regularity. As concluded, the temperature-induced RI measurement error could be ignored by using a different interrogation method.

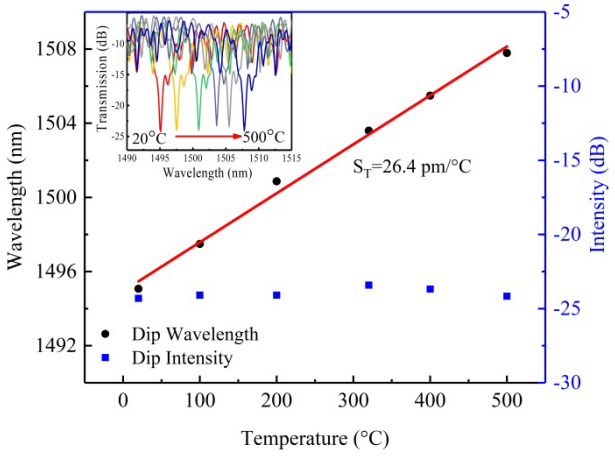

FIGURE 8. Resonance dip wavelength shift and intensity variation of the proposed sensor (L=5 mm) corresponds to temperature. Insert Transmission spectra evolution of the proposed sensor corresponds to temperature.

As shown in the experimental results above, the visibility of the resonance dips was found to shallow with the surrounding RI increase, but the wavelength of the resonance dips hardly changed. Similarly, when the temperature did change, the wavelength of the resonance dips shifted significantly, but the visibility showed no evident change. Therefore, it is a sensible way to use the inornate HCF as a gas RI sensor to overcome the temperature cross-sensitivity problem. More meaningfully, this inornate HCF-based gas RI sensor had a maximum sensitivity of 2,236.1 dB/RIU for an HCF of length 5 mm, the sensitivity could continue to be improved by increasing the length of the HCF.

IV. CONCLUSION

In summary, a novel and simple ultrasensitive gas RI sensor was proposed and demonstrated by splicing a section of HCF between two sections of SMF. We theoretically investigated the transmission spectra characteristics and resonance intensity variations to the gas RI, and found that the intensity sensitivity of inornate HCF is higher than that of coated HCF. We also experimentally proved that the gas RI sensitivity could substantially enhanced by increasing the length of the HCF. A sample with a 5 mm HCF length achieved the highest sensitivity of 2236.1 dB/RIU in the range of gas RI from 1.000 to 1.002. Moreover, the temperature cross-sensitivity was resolved through wavelength interrogation. The proposed sensor exhibited the advantages of simple structure, easy fabrication, and appears to have potential applications in chemistry research.

REFERENCES

[1] N. Liu, M. L. Tang, M. Hentschel, H. Giessen, and A. P. Alivisatos, "Nanoantenna-enhanced gas sensing in a single tailored nanofocus," *Nature Mater.*, vol. 10, no. 8, pp. 631–636, Aug. 2011, doi: 10.1038/NMAT3029.

[2] P. B. Corkum, C. Rolland, and T. Srinivasan-Rao, "Supercontinuum generation in gases," *Phys. Rev. Lett.*, vol. 57, no. 18, pp. 2268–2271, Nov. 1986.

[3] S. Asaduzzaman and K. Ahmed, "Proposal of a gas sensor with high sensitivity, birefringence and nonlinearity for air pollution monitoring," *Sens. Bio-Sensing Res.*, vol. 10, pp. 20–26, Sep. 2016, doi: 10.1016/j.sbsr.2016.06.001.

[4] Z. Li, L. Hou, L. Ran, J. Kang, and J. Yang, "Ultra-sensitive fiber refractive index sensor with intensity modulation and self-temperature compensation," *Sensors*, vol. 19, no. 18, p. 3820, Sep. 2019, doi: 10.3390/s19183820.

[5] L. Jiang, L. Zhao, S. Wang, J. Yang, and H. Xiao, "Femtosecond laser fabricated all-optical fiber sensors with ultrahigh refractive index sensitivity: Modeling and experiment," *Opt. Exp.*, vol. 19, no. 18, pp. 17591–17598, Aug. 2011, doi: 10.1364/OE.19.017591.

[6] Y. Hu, Y. Hou, A. Ghaffar, and W. Liu, "A narrow groove structure based plasmonic refractive index sensor," *IEEE Access*, vol. 8, pp. 97289–97295, 2020, doi: 10.1109/ACCESS.2020.2993707.

[7] Z. Cao, L. Jiang, S. Wang, P. Wang, F. Zhang, and Y. Lu, "Trench-embedding fiber taper sensor fabricated by a femtosecond laser for gas refractive index sensing," *Appl. Opt.*, vol. 53, no. 6, pp. 1028–1032, 2014, doi: 10.1364/AO.53.001028.

[8] Y. Zhang, W. G. Zhang, Y. X. Zhang, L. Yu, L. X. Kong, T. Y. Yan, and L. Chew, "Parabolic-cylinder-like long-period fiber grating sensor based on refractive index modulation enhancement effect," *Appl. Opt.*, vol. 58, no. 7, pp. 1772–1777, 2019, doi: 10.1364/AO.58.001772.

[9] J. Dong, M. Sang, S. Wang, T. Xu, L. Yang, Y. Han, F. Zhao, and T. Liu, "Refractive index sensor based on graphene oxide-coated long-period fiber grating inscribed in a two-mode fiber," *IEEE Access*, vol. 8, pp. 109028–109037, 2020, doi: 10.1109/ACCESS.2020.3001375.

[10] J. Madrigal, D. Barrera, and S. Sales, "Refractive index and temperature sensing using inter-core crosstalk in multicore fibers," *J. Lightw. Technol.*, vol. 37, no. 18, pp. 4703–4709, Sep. 15, 2019, doi: 10.1109/JLT.2019.2917629.
[11] L. Sun, Z. H. Yuan, T. S. Huang, Z. Sun, W. F. Lin, Y. Huang, P. Xiao, M. J. Yang, J. Li, and B. O. Guan, "Ultrasensitive sensing in air based on Sagnac interferometer working at group birefringence turning point," *Opt. Exp.*, vol. 27, no. 21, pp. 29501–29509, 2019, doi: 10.1364/OE.27.029501.
[12] M. Quan, J. Tian, and Y. Yao, "Ultra-high sensitivity Fabry–Pérot interferometer gas refractive index fiber sensor based on photonic crystal fiber and Vernier effect," *Opt. Lett.*, vol. 40, no. 21, pp. 4891–4894, 2015, doi: 10.1364/OL.40.004891.
[13] N. M. Y. Zhang, K. Li, N. Zhang, Y. Zheng, T. Zhang, M. Qi, P. Shum, and L. Wei, "Highly sensitive gas refractometers based on optical microfiber modal interferometers operating at dispersion turning point," *Opt. Exp.*, vol. 26, no. 22, pp. 29148–29158, 2018, doi: 10.1364/OE.26.029148.
[14] K. Li, N. Zhang, N. M. Y. Zhang, G. Liu, T. Zhang, and L. Wei, "Ultrasensitive measurement of gas refractive index using an optical nanofiber coupler," *Opt. Lett.*, vol. 43, no. 4, p. 679, Feb. 2018, doi: 10.1364/OL.43.000679.
[15] A. M. Zheltikov, "Ray-optic analysis of the (bio)sensing ability of ring-cladding hollow waveguides," *Appl. Opt.*, vol. 47, no. 3, p. 474, Jan. 2008, doi: 10.1364/AO.47.000474.
[16] H. Sun, H. Luo, X. Wu, L. Liang, Y. Wang, X. Ma, J. Zhang, M. Hu, and X. Qiao, "Spectrum ameliorative optical fiber temperature sensor based on hollow-core fiber and inner zinc oxide film," *Sens. Actuators B, Chem.*, vol. 245, pp. 423–427, Jun. 2017, doi: 10.1016/j.snb.2017.01.151.
[17] R. Gao, D.-F. Lu, J. Cheng, Y. Jiang, L. Jiang, and Z.-M. Qi, "Humidity sensor based on power leakage at resonance wavelengths of a hollow core fiber coated with reduced graphene oxide," *Sens. Actuators B, Chem.*, vol. 222, pp. 618–624, Jan. 2016, doi: 10.1016/j.snb.2015.08.108.
[18] M. Hou, J. He, X. Xu, Z. Li, Z. Zhang, K. Guo, S. Ju, and Y. Wang, "Antiresonant reflecting guidance and Mach-Zender interference in cascaded hollow-core fibers for multi-parameter sensing," *Sensors*, vol. 18, no. 12, p. 4140, Nov. 2018, doi: 10.3390/s18124140.
[19] D. Liu, R. Kumar, F. Wei, W. Han, A. K. Mallik, J. Yuan, C. Yu, Z. Kang, F. Li, Z. Liu, H.-Y. Tam, G. Farrell, Y. Semenova, and Q. Wu, "Highly sensitive twist sensor based on partially silver coated hollow core fiber structure," *J. Lightw. Technol.*, vol. 36, no. 17, pp. 3672–3677, Sep. 1, 2018, doi: 10.1109/JLT.2018.2842111.
[20] L. A. Herrera-Piad, I. Hernández-Romano, D. A. May-Arrioja, V. P. Minkovich, and M. Torres-Cisneros, "Sensitivity enhancement of curvature fiber sensor based on polymer-coated capillary hollow-core fiber," *Sensors*, vol. 20, no. 13, p. 3763, Jul. 2020, doi: 10.3390/s20133763.
[21] R. Gao, D.-F. Lu, J. Cheng, Y. Jiang, L. Jiang, and Z.-M. Qi, "Optical displacement sensor in a capillary covered hollow core fiber based on anti-resonant reflecting guidance," *IEEE J. Sel. Topics Quantum Electron.*, vol. 23, no. 2, pp. 193–198, Mar. 2017, doi: 10.1109/JSTQE.2016.2544705.
[22] M. Huang, C. Yang, B. Sun, Z. Zhang, and L. Zhang, "Ultrasensitive sensing in air based on graphene-coated hollow core fibers," *Opt. Exp.*, vol. 26, no. 3, p. 3098, Feb. 2018, doi: 10.1364/OE.26.003098.
[23] P. Jaworski, P. Kozioł, K. Krzempek, D. Wu, F. Yu, P. Bojęś, G. Dudzik, M. Liao, K. Abramski, and J. Knight, "Antiresonant hollow-core fiber-based dual gas sensor for detection of methane and carbon dioxide in the near- and mid-infrared regions," *Sensors*, vol. 20, no. 14, p. 3813, Jul. 2020, doi: 10.3390/s20143813.
[24] H. Gao, Y. Jiang, L. Zhang, Y. Cui, Y. Jiang, J. Jia, and L. Jiang, "Antiresonant mechanism based self-temperature-calibrated fiber optic Fabry–Pérot gas pressure sensors," *Opt. Exp.*, vol. 27, no. 16, p. 22181, Aug. 2019, doi: 10.1364/OE.27.022181.
[25] M. Hou, F. Zhu, Y. Wang, Y. P. Wang, C. R. Liao, S. Liu, and P. X. Lu, "Antiresonant reflecting guidance mechanism in hollow-core fiber for gas pressure sensing," *Opt. Exp.*, vol. 24, no. 24, pp. 27890–27898, 2016, doi: 10.1364/OE.24.027890.
[26] S. Liu, Y. Wang, M. Hou, J. Guo, Z. Li, and P. Lu, "Anti-resonant reflecting guidance in alcohol-filled hollow core photonic crystal fiber for sensing applications," *Opt. Exp.*, vol. 21, no. 25, pp. 31690–31697, 2013, doi: 10.1364/OE.21.031690.
[27] C. H. Lai, B. W. You, J. Y. Lu, T. A. Liu, J. L. Peng, C. K. Sun, and H. C. Chang, "Modal characteristics of antiresonant reflecting pipe waveguides for terahertz waveguiding," *Opt. Exp.*, vol. 18, no. 1, pp. 309–322, 2010, doi: 10.1364/OE.18.000309.
[28] M. Szpulak, T. Martynkien, and W. Urbanczyk, "Effects of hydrostatic pressure on phase and group modal birefringence in microstructured holey fibers," *Appl. Opt.*, vol. 43, no. 24, pp. 4739–4744, 2004, doi: 10.1364/AO.43.004739.
[29] L. Jin, B.-O. Guan, and H. Wei, "Sensitivity characteristics of Fabry–Pérot pressure sensors based on hollow-core microstructured fibers," *J. Lightw. Technol.*, vol. 31, no. 15, pp. 2526–2532, Aug. 2013, doi: 10.1109/JLT.2013.2269136.
[30] K. P. Birch and M. J. Downs, "An updated Edlén equation for the refractive index of air," *Metrologia*, vol. 30, no. 3, pp. 155–162, Jan. 1993, doi: 10.1088/0026-1394/30/3/004.

MAOXIANG HOU was born in Hunan, China, in 1990. He received the M.S. degree in applied physics from Northeastern University, Shenyang, China, in 2011, and the Ph.D. degree in optics from the Huazhong University of Science and Technology, in 2016. He is currently a Lecturer with the State Key Laboratory of Precision Electronic Manufacturing Technology and Equipment, School of Electromechanical Engineering, Guangdong University of Technology, Guangzhou, China. His main research interests include femtosecond laser micromachining, fiber Bragg gratings, and optical fiber sensing.

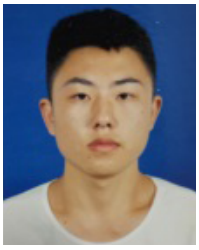

NENG WANG was born in Hubei, China, in 1997. He received the bachelor's degree from Hubei Polytechnic University, Hubei, in 2019. He is currently pursuing the master's degree with the Guangdong University of Technology, Guangzhou, China.

JIANGUO MA was born in Jiangxi, China, in 1997. He received the bachelor's degree from the Nanchang Institute of Technology, Nanchang, China, in 2019. He is currently pursuing the master's degree with the Guangdong University of Technology, Guangzhou, China.

YUN CHEN received the B.S. and Ph.D. degrees in mechanical engineering from Central South University, Changsha, China, in 2009 and 2014, respectively. From 2016 to 2017, he was a Visiting Scholar with the Georgia Institute of Technology. From 2017 to 2019, he was a Hong Kong Scholar Postdoctoral Fellow with The Chinese University of Hong Kong. He is currently a Professor with the State Key Laboratory of Precision Electronic Manufacturing Technology and Equipment, School of Electromechanical Engineering, Guangdong University of Technology. He has authored more than 30 peer-reviewed articles and holds more than 60 patents. His research interests include semiconductor processing technology, microelectronics packaging technology, and equipment development.

XIN CHEN (Member, IEEE) received the Ph.D. degree in mechanical engineering from the Huazhong University of Science and Technology, Wuhan, China, in 1995. He is currently a Professor with the School of Electromechanical Engineering, Guangdong University of Technology, Guangzhou, China. His research interests include mechanical dynamics, IC packaging equipment technology, and device development.